JOURNAL OF Applied Polymer SCIENCE

Crystallization Behavior of Poly(*p*-dioxanone)-PU/Montmorillonite Nanocomposites Prepared by Chain-Extending Reaction

Yan Zhou,[1,2] Jing-Jing Zhang,[1] Ying Niu,[1] Cai-Li Huang,[1] Ke-Ke Yang[1]

[1]Center for Degradable and Flame-Retardant Polymeric Materials (SC Key Laboratory), National Engineering Laboratory of Eco-Friendly Polymeric Materials (Sichuan), College of Chemistry, State Key Laboratory of Polymer Materials Engineering, Sichuan University, Chengdu 610064, China

[2]Chemistry and Chemical Engineering Department, Mianyang Normal University, Mianyang 621000, China

Correspondence to: K.-K. Yang (E-mail: kkyangscu@126.com)

ABSTRACT: Organo-modified montmorillonites and poly(*p*-dioxanone) (PPDO) diol prepolymers were used to prepare Poly(*p*-dioxanone)-PU/organic montmorillonite (PPDO-PU/OMMT) nanocomposites by chain-extending reaction. The crystallization behavior and spherulitic morphology of PPDO-PU/OMMT nanocomposites were investigated by WXRD, differential scanning calorimetry, and polarized optical microscopy. The results show that the regularity of the chain structure plays a dominant role during the crystallization process rather than that of OMMT content and its dispersion status in PPDO matrix. With similar molecular weight and same OMMT content, PPDO-PU/OMMT nanocomposite, which derived from lower molecular weight PPDO prepolymer, exhibits lower crystallization rate, melting point, and crystallinity. The influence of the clay content on the crystallization behavior highly depends on its dispersing state. The nucleating effect of OMMT can be only observed at high loading percentage. For the nanocomposites with low clay loading percentage, the retarding effect of exfoliated platelets on the chain-ordering into crystal lamellae became the key factor. © 2012 Wiley Periodicals, Inc. J. Appl. Polym. Sci. 000: 000–000, 2012

KEYWORDS: biodegradable; nanocomposites; crystallization; structure–property relations

Received 20 July 2011; accepted 7 March 2012; published online
DOI: 10.1002/app.37641

INTRODUCTION

Poly(*p*-dioxanone) (PPDO), a typical aliphatic poly(ether-ester) with excellent biodegradability, bioabsorbability, biocompatibility, and mechanical performance, is considered as a good candidate both in biomedical application and universal uses.[1–7] Recently, more and more reports concerned the modification of this polymer to improve the thermal stability, increase the crystallization rate, enhance the melt viscosity, and repress the hydrolyze tendency. Various techniques such as copolymerization,[8–29] chain extending,[30–34] blending[35–39] and adding nanofillers[40–46] were attempted for these purposes.

In our previous work, chain-extending technique was used successfully to produce high-molecular-weight PPDO with highly improved thermal stability, mechanical properties, and rheological behavior, whereas the crystallization rate and crystallinity of the products decrease.[32–34] Several PPDO/clays nanocomposites were also developed by *in situ* ring-opening polymerization. Significant improvement on mechanical properties and rheological behavior were also achieved in nanocomposites.[41–44] In some cases, clays were found acting as nucleating agent and increase the crystallization rate of PPDO dramatically. In this work, we combine these two techniques to prepare PPDO-PU/OMMT nanocomposite by chain-extending reaction, aimed to improve the processability and performance of this polymer. As we known, the insert of chain-extenders disturb the regularity of PPDO polymer chains, and inevitably, the depression of the crystallizability was observed. Otherwise, incorporating different aspect and scale nanofillers into PPDO and its different dispersion morphology influence the crystallization behavior of nanocomposites significantly. In the present work, WXRD, differential scanning calorimetry (DSC), and POM were employed to disclose the feature of crystallization behavior affected by those two factors.

EXPERIMENTAL

Materials

p-Dioxanone (PDO), provided by the Pilot Plant of the Center for Degradable and Flame-Retardant Polymeric Materials (Chengdu, China), was dried over CaH_2 and distilled under reduced pressure. Stannous octoate ($SnOct_2$) (≥95%) from Sigma (USA) was used as received. 1,4-butanediol (BD) was

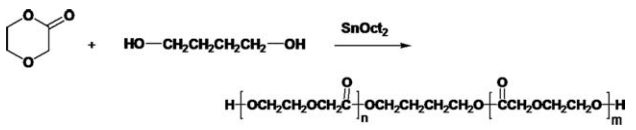

Scheme 1. Synthesis route of PPDO diol prepolymers.

purchased from Zhiyuan Chemical Company (Tianjin, China) and was used after drying. HDI was obtained from J&K Chemical Ltd (Shanghai, China), Natural sodium montmorillonite (MMT-Na) was supplied by Shanghai Chemical Co. (Shanghai, China), and other reagents were purchased from Sitong Chemical Company (Chengdu, China) and used without further purification.

Preparation of PPDO-PU/OMMT Nanocomposites

Synthesis of PPDO Diol Prepolymers. Scheme 1 shows the synthetic route of PPDO diol prepolymer, and the synthetic procedure was followed our previous article.[34] The products were named as $PPDO_n$; here, the subscript "n" refers to the molar feed ratio of PPDO/BD, and three different feed ratios (20, 40, and 100) were chosen in the present work.

Preparation of PPDO-PU by Chain Extending of PPDO Diol Prepolymer. Synthetic approach of PPDO-PU by Chain extending of PPDO diol prepolymer was illustrated in Scheme 2, and the synthetic procedure was followed our previous article.[34] The products were named as $PPDO_n$-PU, and the feed ratio and the molecular weight of samples were listed in Table I.

Preparation of PPDO-PU/OMMT Nanocomposites by Chain Extending of PPDO Diol Prepolymer and OMMT. Preparation procedure of PPDO-PU/OMMT nanocomposites was followed our previous article.[40] The product nanocomposites were abbreviated as $PPDO_n$-PU/a%OMMT; here, the lowercase "a" refers to the OMMT loading percentage in PPDO-PU/OMMT nanocomposite.

Characterization

Intrinsic Viscosity. As the conventional solvents such as chloroform and tetrahydrofuran used in GPC measurements cannot dissolve the PPDO-PU/OMMT nanocomposites and PPDO with higher molecular weights, only the intrinsic viscosity [η] of the resulting composites were measured in phenol/1,1,2,2-tetrachloroethane (1 : 1 v/v) solution using an Ubbelohde viscometer maintained at 30°C.

Transmission Electron Microscopy. Transmission electron microscopy (TEM) photographs were obtained with a Philips CM200 Transmission Electron Microscope, which was operated at an accelerated voltage of 120 kV.

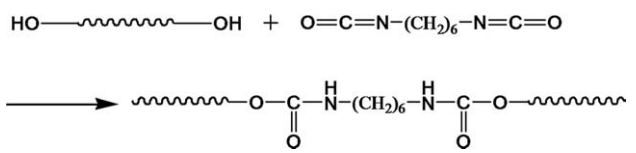

Scheme 2. The process of chain extending reaction of PPDO diol prepolymers with HDI.

Wide-Angle X-ray Diffraction Analysis. Wide-angle X-ray diffraction (WAXD) analysis was performed on a Philips X'pert diffractometer, which had an X-ray generator of 3-kW, graphite monochromatic, Cu Kα radiation (wavelength = 1.5406 Å) and was operated at 40 kV and 20 mA. WAXD patterns of various PPDO-PU/OMMT nanocomposites were evaluated from films. The samples were scanned at room temperature from 2° to 40° at a scanning rate of 2°/min.

Differential Scanning Calorimetry. Nonisothermal crystallization was performed with TA Q100 (TA instruments, USA), and the sample in sealed aluminum pan under nitrogen atmosphere. The samples were cooled to −50°C from room temperature, and then heated to 140°C at a heating rate of 5°C/min, kept for 5 min to eliminate the thermal history, then cooled to −50°C at a cooling rate of 5°C/min. The samples were again heated up to 140°C at the same rate. The glass transition temperature (T_g), the crystallization temperature (T_c), and the melting temperature (T_m) were obtained from the thermogram.

Isothermal Crystallization Kinetics. Isothermal crystallization was performed after melting at 140°C for 5 min to erase all previous thermal history and then was quenched (at a nominal rate of 80°C/min) to the isothermal crystallization temperature T_c. The crystallization process was then followed. The sample was held at T_c for the required time to develop to the maximum possible crystallinity degree. Data taken during this isothermal run were used to perform the Avrami analysis.

The Avrami's equation has been proposed to analyze the isothermal crystallization calorimetric data obtained by DSC.[47]

$$1 - X_t = \exp(-kt^n) \quad (1)$$

where n is the Avrami exponent, k is the Avrami rate constant, X_t is the relative crystallinity at time t, and X_t was calculated by

Table I. Characteristics of Samples Prepared

Samples	n(PDO) : n(BD)	OMMT content (%)	[η] (dL/g)
$PPDO_{40}$-PU[a]	40	0	1.47
$PPDO_{40}$-PU/1%OMMT[a]	40	1	1.48
$PPDO_{40}$-PU/3%OMMT[a,b,c]	40	3	1.69
$PPDO_{40}$-PU/5%OMMT[a]	40	5	1.46
$PPDO_{20}$-PU/3%OMMT[a]	20	3	2.00
$PPDO_{100}$-PU/3%OMMT[a,b,c]	100	3	1.67
$PPDO_{40}$-PU[d]	40	0	1.62
$PPDO_{40}$-PU/1%OMMT[d]	40	1	1.41
$PPDO_{40}$-PU/3%OMMT[d]	40	3	1.58
$PPDO_{40}$-PU/3%OMMT[d]	40	3	1.80
$PPDO_{20}$-PU/3%OMMT[c,d]	20	3	1.65
$PPDO_{100}$-PU/3%OMMT[d]	100	3	1.80
Homo-PPDO[c]	—	—	1.70

[a]Samples for DSC measurement, [b]Samples for TEM measurement, [c]Samples for XRD measurement, [d]Samples for POM measurement.

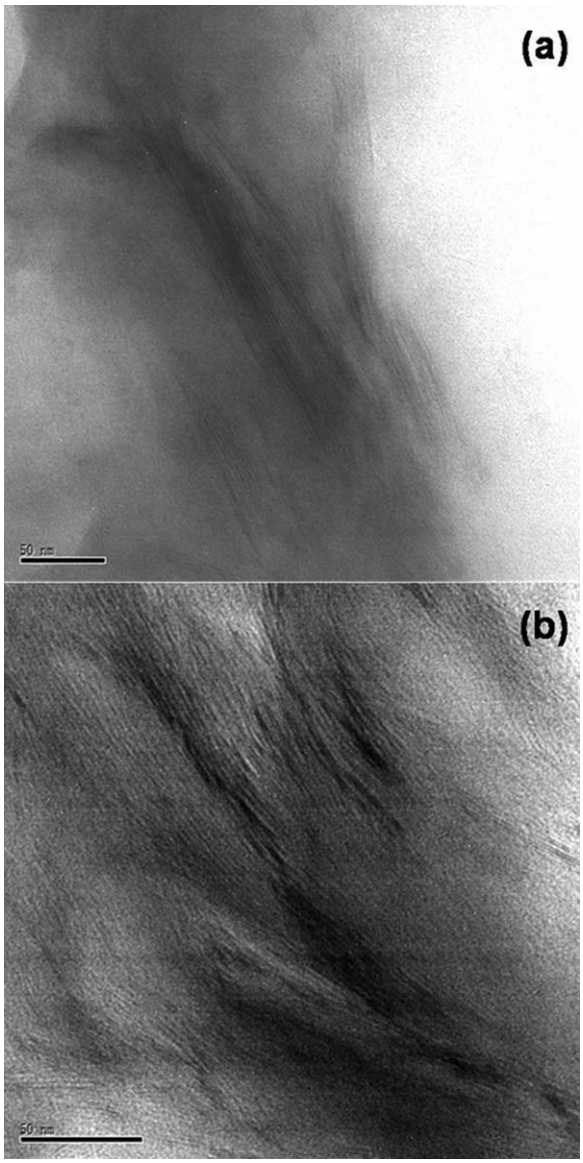

Figure 1. TEM micrographs of various PPDO-PU/OMMT nanocomposites: (a) $PPDO_{40}$-PU/3%OMMT; (b) $PPDO_{100}$-PU/3%OMMT.

integration of the exothermic peak during the isothermal crystallization process, according to the following equation:

$$X_t = \frac{\int_0^t (dH_c/dt)/dt}{\int_0^\infty (dH_c/dt)/dt} \quad (2)$$

where (dH_c/dt) is DSC heat flow. Setting eq. (1) equal to 0.5, the crystallization half-time, $t_{1/2}$, defined as the time to a relative crystallinity of 50%, can be obtained:

$$t_{1/2} = (\ln 2/k)^{1/n} \quad (3)$$

In general, both k and n depend on the nucleation and growth mechanisms of spherulites. To convert conveniently with the operation, eq. (1) can be transformed into:

$$\lg[-\ln(1 - X_t)] = \lg k + n \lg t \quad (4)$$

The Avrami exponent, n, could be directly obtained using eq. (4) from the slope of the best-fitting line. Finally, the composite rate constant, k, can be evaluated either from the intercept or calculated using eq. (3).

Polarized Optical Microscopy. Polarized optical microscopy (POM) studies were carried out with a Nikon ECLIPSE LV100POL microscope in conjunction with a hot stage (HSC621 V). The specimens were heated to 140°C on a hot stage and held at that temperature for 5 min and then quickly cooled to crystallization temperature. The growth of spherulites was recorded on a VCR, and the growth rate data were measured from time-lapsed frames of spherulitic fronts; photographs were taken by a digital camera.

RESULTS AND DISCUSSION

Table I listed all the samples with different MMT content and different chain structure employed in present work, which were prepared followed our previous work.[32,34] As we have investigated the structure of the products produced by this approach by FTIR, NMR. and TGA systematically, here, we just supplied the information of the feed ratio and molecular weight of all samples. Compared with neat PPDO, urethane bonds and nanofillers were introduced into PPDO-PU/OMMT nanocomposites. To reveal the influence of these two factors on the crystallization behavior of PPDO-PU/OMMT nanocomposites, two different series of PPDO-PU/OMMT composites were designed and well prepared, one is that with same OMMT content but different urethane bonds content, and the other is that with same urethane bonds content but different OMMT content.

TEM observation was performed to confirm the microstructure of the nanocomposites. Here, TEM images of $PPDO_{100}$-PU/3%OMMT and $PPDO_{40}$-PU/3%$OMMT_3$ were shown in Figure 1 as examples, in which the gray areas represent the silicate layers in the PPDO matrix. TEM images revealed the layered montmorillonite disperse in the PPDO matrix with an intercalated-

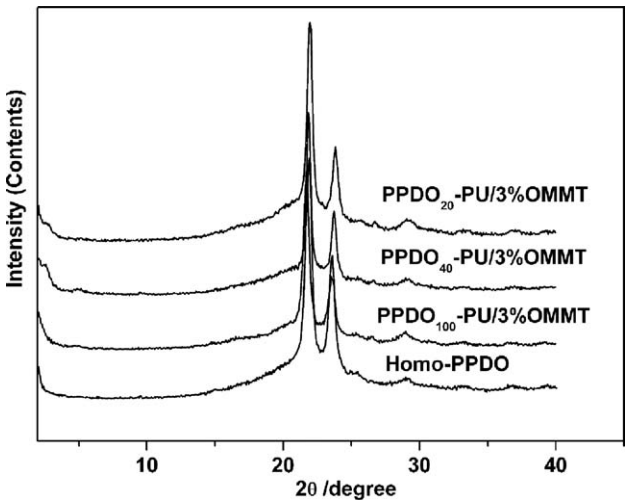

Figure 2. WXRD curves of PPDO and PPDO-PU/OMMT.

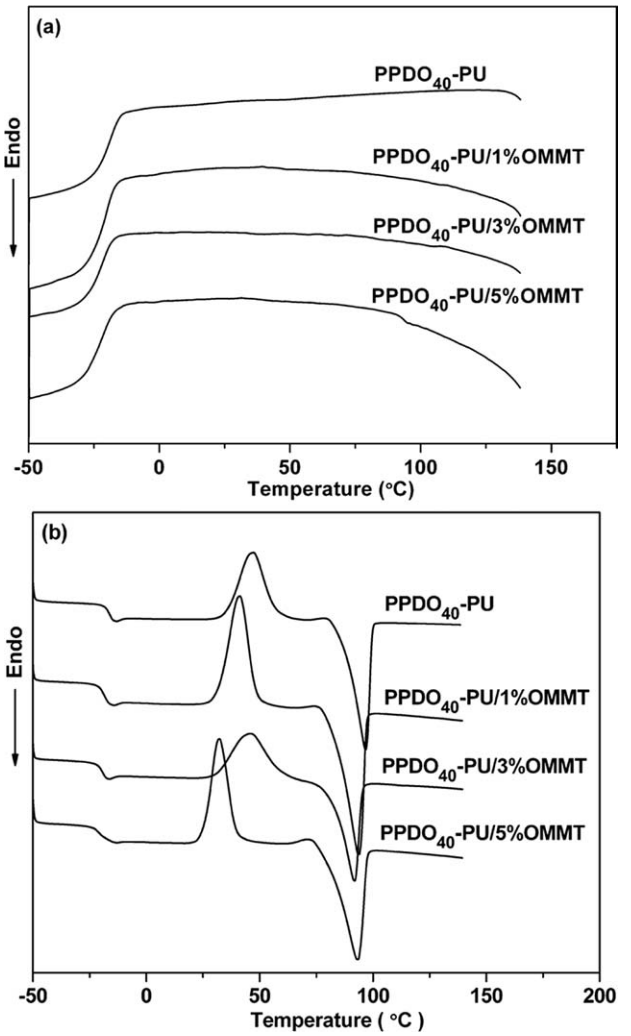

Figure 3. DSC curves of different $PPDO_{40}$-PU/OMMT nanocomposites with different OMMT content: (a) the cooling scan after eliminating the thermal history; (b) the second heating scan from −50 to 140°C.

exfoliated coexistence structure, and most likely in intercalated state, especially in $PPDO_{100}$-PU/3%OMMT. It may ascribe to that the $PPDO_{100}$-PU/3%OMMT was derived from high-molecular-weight propolymer $PPDO_{100}$, which was more difficult to swollen into the gallery of OMMT layers. With the increase of OMMT content or decrease of urethane bonds content, the OMMT is more likely tend to disperse with intercalated structure.[40]

XRD Characterization

The influence of chain structure and the OMMT content on the crystallization behaviors of PPDO-PU/OMMT nanocomposites were described in detail in this work. Figure 2 gives the information of crystal structure of PPDO matrix, and it clearly shows that various PPDO-PU/OMMT nanocomposites have the same characteristic diffraction peaks at $2\theta = 21.9$, 23.7, and 29.4 as pure PPDO does, which attribute to the reflection of (210), (020), and (310), respectively.[45] The results suggest that there is no significant effect of the OMMT on the crystal structure of the matrix of PPDO, the same phenomenon also was found in the PPDO/OMMT[43] and PPDO/OVMT nanocomposites.[44] However, we cannot observe the intercalated OMMT structure in the XRD; this phenomenon may be caused by the low content of the OMMT.

Nonisothermal Crystallization Behavior of PPDO-PU/OMMT Nanocomposites

DSC was used to record the thermal behavior of PPDO-PU/OMMT nanocomposites during the cooling scans and the followed heating scans. Figure 3 shows the DSC curves of a series of PPDO-PU/OMMT nanocomposites, and the relevant data were summarized in Table II. These four samples had similar molecular weight ($[\eta] = 1.5$–1.7 dL/g) and chain structure but different OMMT content. The influence of OMMT and its loading percentage on the crystallization behaviors of the nanocomposites were discussed firstly.

Figure 3(a) illustrates the cooling scans from 140°C to −50°C after eliminating the thermal history, and no crystallization exotherm peak can be detected in this run for all samples; nevertheless, it appears in the following heating scan [Figure 3(b)]. In our previous work, MMT with intercalated structure in PPDO matrix could act as nucleating agent during the crystallization process, and it greatly increased the crystallization rate.[41,43] However, apparently, the incorporation of OMMT into PPDO-PU depresses the crystallization of nanocomposites, which results the decrease of the melting temperature (T_m) and crystallinity. Compared with PPDO homopolymer, PPDO-PU exhibits very weak crystallinity because the irregularity of polymer chains; furthermore, OMMT layers also act as obstacle to the folding of polymer chains. The nucleating effect caused by intercalated layers could be ignored during the crystallization process, which is dominant by crystal growth rate, especially in low OMMT loading percentage. Therefore, the nanocomposites exhibit poorer crystallizability than PPDO-PU copolymers.

Figure 4 shows the DSC curves of PPDO-PU/OMMT nanocomposites ($[\eta] = 1.7$–2.0 dL/g) with same OMMT content (3%)

Table II. DSC Data of Different PPDO-PU/OMMT Nanocomposites

Samples	T_g (°C)	T_c (°C)	T_m (°C)	ΔH_m (J/g)	C^a
$PPDO_{40}$-PU	−16	47	97	51.1	36.2
$PPDO_{40}$-PU/1%OMMT	−18	41	94	47.4	33.6
$PPDO_{40}$-PU/3%OMMT	−19	46	92	42.3	30.0
$PPDO_{40}$-PU/5%OMMT	−21	32	93	48.8	34.6

[a]Crystallinity of the samples determined by first and second heating scan, the heat of fusion ΔH_m^0 for 100% crystalline PPDO has been determined by Wunderlich and coworkers[48] as 141 J/g.

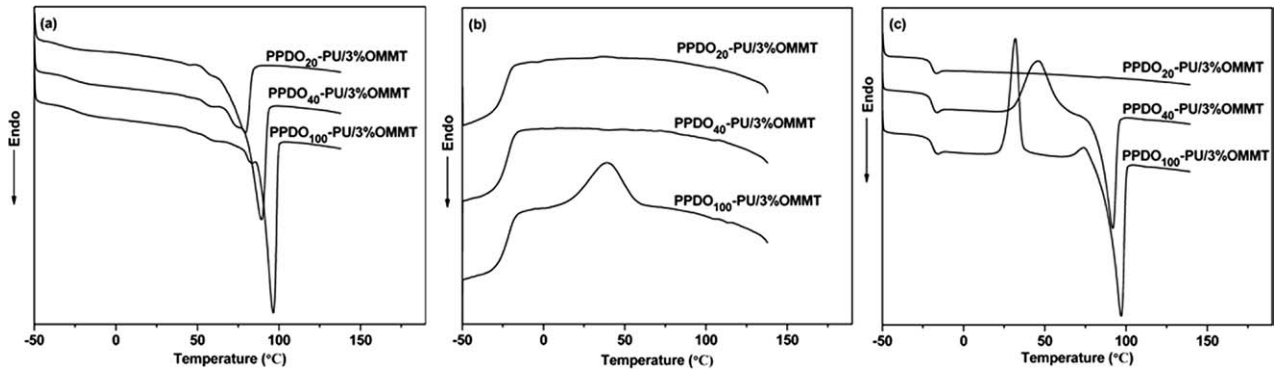

Figure 4. DSC curves of different PPDO-PU/3%OMMT nanocomposites: (a) the first heating scan from −50 to 140°C; (b) the cooling scan after eliminating the thermal history; and (c) the second heating scan from −50 to 140°C.

but different chain structure, and the characteristic parameters are summarized in Table III. Figure 4(a) illustrates the first heating scans of samples from −50°C to 140°C, without eliminating the thermal history. Melting peaks were observed in all the samples, which indicated that all the samples have the ability of crystallization, although the melting temperature decreased with the increase of urethane group content. Figure 4(b) displays the cooling scans from 140°C to −50°C after eliminating the thermal history, and the crystallization exotherm peak appeared only in the curve of $PPDO_{100}$-PU/3%OMMT. In the second heating run [Figure 4(c)], still no crystallization exotherm peak could be detected in $PPDO_{20}$-PU/3%OMMT under present scan rate. In conclusion, the crystallizability of nanocomposite decreased with the increase of urethane group content. It may be ascribed to the breakage of chain regularity by introduce the chain extender, and the close packing capability of polymer chains decrease sharply with the increase of urethane group content. As a result, the formation of unperfected crystal leads to low T_m. This phenomenon is quite corresponding to that of PPDO-PU system.[34]

Isothermal Crystallization Kinetics

Figure 5 presents the isothermal crystallization analysis exothermal diagrams of different PPDO-PU/OMMT nanocomposites. Obviously, with the isothermal crystallization temperature (T_c) increased, the exothermal peaks shift to longer time which indicated that a progressively slower crystallization rate as T_c increased. The relative crystallinity X_t versus t in isothermal crystallization were also shown in Figure 5

Figure 6 shows the plot of $\lg[-\ln(1 - X_t)]$ versus $\lg t$ for different nanocomposites. The k and n values could be directly obtained using eq. (4) from the intercept and slope of the best-fitting line (correlation coefficients were greater than 0.998 in all cases). In the present work, we focus only on primary crystallization. Several crystallization parameters $t_{1/2}$, k, and n are summarized in Table IV. The isothermal crystallization rates of all PPDO-PU/OMMT nanocomposite samples conducted by $1/t_{1/2}$ decrease as T_c increases in the chosen temperature range. But it did not increase with the increasing the OMMT content monotonously, for example, $PPDO_{40}$-PU/3%OMMT had the lowest isothermal crystallization rate at 45 °C. In fact, at low OMMT loading percentage, a relative high proportion OMMT layers disperse in exfoliate morphology, and the nucleating effect caused by intercalated layers could be ignored during the crystallization process otherwise the obstacle effect on chain folding was dominant the spherulite growth. While the OMMT loading percentage increased to high content (5%), and it was most likely to disperse with intercalated structure, the nucleating effect of OMMT was pronounced. Consequently, $PPDO_{40}$-PU/3%OMMT exhibits the lowest crystallization rate.

The crystallization rate parameter k can also be approximately described as follows:

$$k^{\frac{1}{n}} = A \cdot e^{-\frac{\Delta E_a}{RT_C}} \tag{5}$$

where A is a temperature-independent pre-exponential factor; E_a is a total activation energy, which consists of the transport activation energy E^* and the nucleation activation energy F (E^*

Table III. DSC Data of Different PPDO-PU/OMMT Nanocomposites with Different Chain Structure

	The first heating scan			Cooling scan		The second heating scan					
Samples	T_m (°C)	ΔH_m (J/g)	C_1[a]	T_c (°C)	ΔH_c (J/g)	T_g (°C)	T_c (°C)	ΔH_c (J/g)	T_m (°C)	ΔH_m (J/g)	C_2[a]
$PPDO_{20}$-PU/3%OMMT	80	41.9		-	-	−19	-	-	-	-	-
$PPDO_{40}$-PU/3%OMMT	90	33.0	23.4	-	-	−19	46	42.0	92	42.3	29.8
$PPDO_{100}$-PU/3%OMMT	97	62.1	44.1	39	9.9	−19	32	31.2	97	39.5	29.1

Applied Polymer SCIENCE

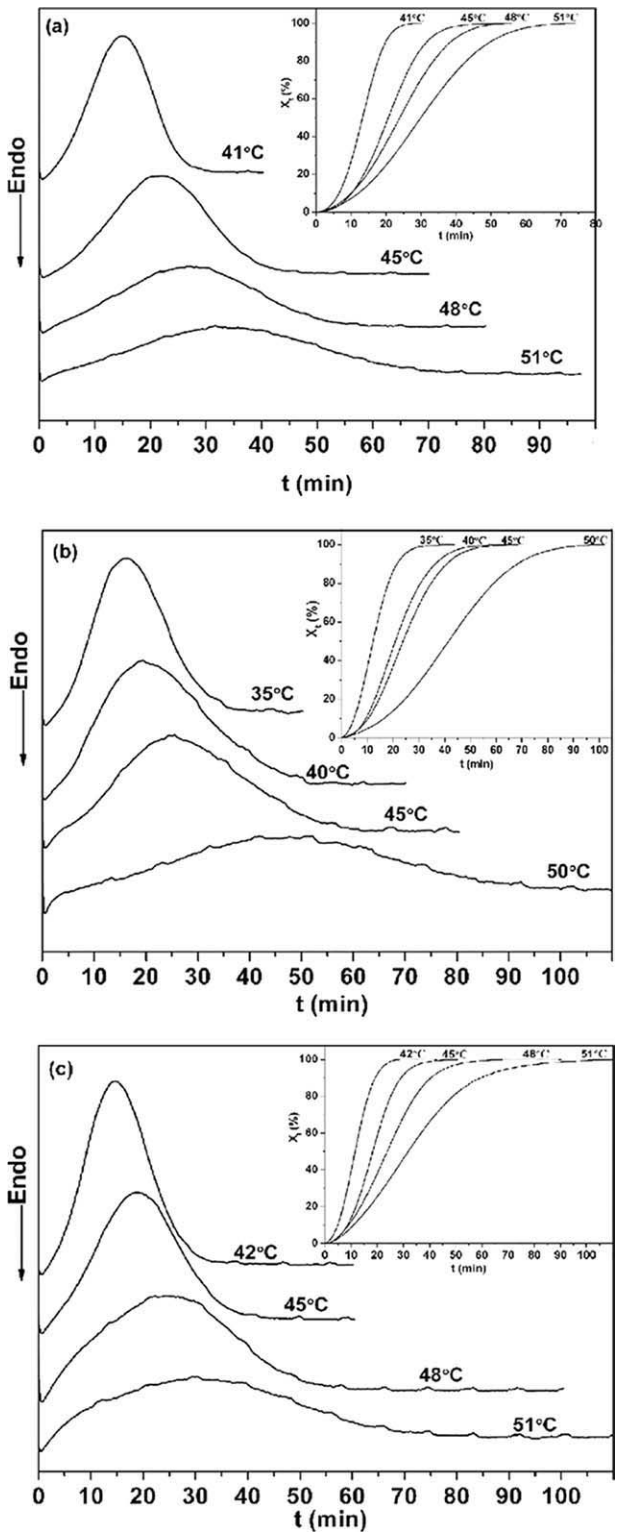

Figure 5. The DSC traces of samples isothermally crystallized at the specified temperature: (a) $PPDO_{40}$-PU/1%OMMT; (b) $PPDO_{40}$-PU/3%OMMT; and (c) $PPDO_{40}$-PU/5%OMMT.

refers to the activation energy required to transport molecular segments across the phase boundary to the crystallization surface and F is the free energy of formation of the critical size crystal nuclei at T_c); and R is the universal gas constant.

Arrhenius plots of $\ln k^{1/n}$ against $1/T$ for $PPDO_{40}$-PU/OMMT are shown in Figure 7, and are approximately linear. The activation energy can be determined from the slope of plots (Table III). Obviously, the lowest absolute ΔE_a value belongs to $PPDO_{40}$-PU/3%OMMT, indicating it more difficult to form crystals.

Spherulitic Morphology of PPDO-PU/OMMT Nanocomposites

To elucidate the relationship of chain structure and spherulitic morphologies, spherulites growing process and the

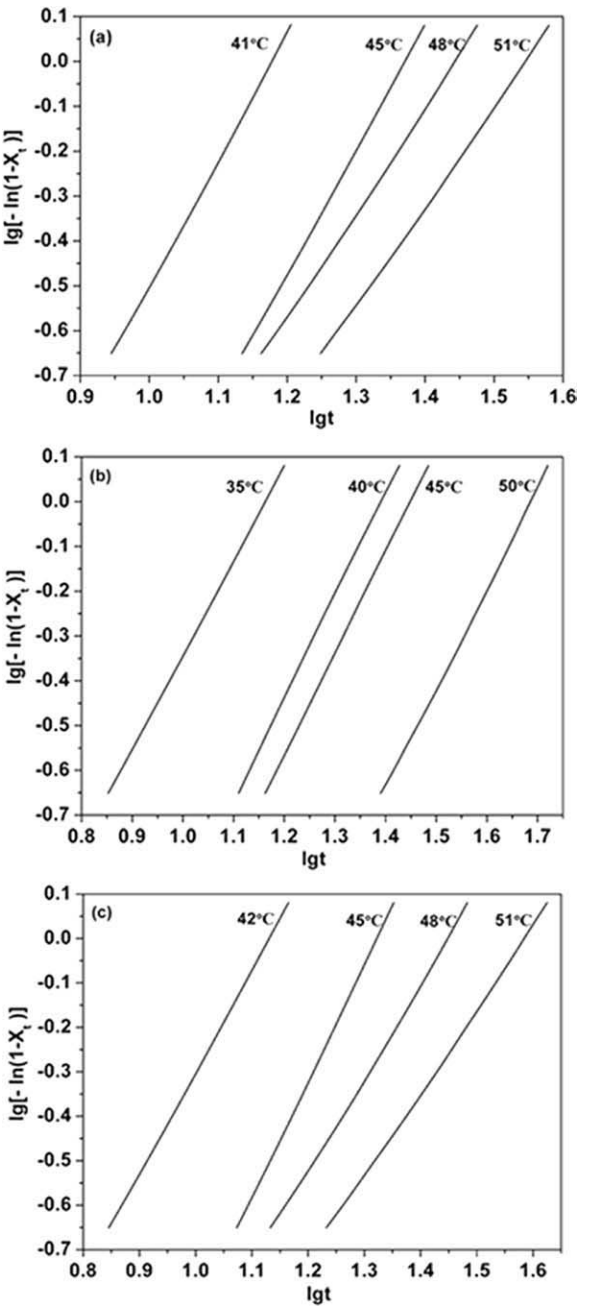

Figure 6. Avrami plots of PPDO-PU/OMMT at different temperatures: (a) $PPDO_{40}$-PU/1%OMMT; (b) $PPDO_{40}$-PU/3%OMMT; (c) $PPDO_{40}$-PU/5%OMMT.

Table IV. Relevant Data of Isothermal Crystallization of PPDO-PU/OMMT

Sample	T_c (°C)	$T_{1/2}$ (min)	k (min^{-n})	n	ΔE_a (kJ/mol)
$PPDO_{40}$-PU/1%OMMT	41	13.28	4.7×10^{-4}	2.82	−70
	45	20.62	1.3×10^{-4}	2.83	
	48	23.91	4.1×10^{-4}	2.35	
	51	29.92	3.7×10^{-4}	2.22	
$PPDO_{40}$-PU/3%OMMT	35	12.25	3.5×10^{-3}	2.11	−62
	40	20.89	6.3×10^{-4}	2.30	
	45	23.85	4.9×10^{-4}	2.23	
	50	41.51	1.7×10^{-4}	2.18	
$PPDO_{40}$-PU/5%OMMT	42	11.56	2.5×10^{-3}	2.30	−96
	45	18.31	3.3×10^{-4}	2.63	
	48	23.79	9×10^{-4}	2.10	
	51	31.82	1.1×10^{-3}	1.88	

superstructural morphologies of PPDO-PU/OMMT nanocomposite were studied by POM, and unloaded PPDO-PU prepared by chain-extending reaction was studied for compare. The isothermal crystallization was conducted in a temperature range from 40°C–70 °C. Figure 8 shows the spherulitic morphologies of PPDO-PU/3%OMMT ([η] = 1.7–1.8 dL/g) at 50°C. Comparatively, $PPDO_{20}$-PU/3%OMMT grew quite small spherulites in imperfect texture. Figure 9 shows the radius of the growing spherulites as a function of time at 50°C. In all samples, the spherulite radius increased linearly with time, and the lines are fitted to the experimental data to calculate the slope and growth rate. It is clear that the spherulite growth rate of $PPDO_{100}$-PU/3%OMMT nanocomposites is the fastest and $PPDO_{20}$-PU/3%OMMT is the slowest. The same phenomenon was also found in other temperatures. It identified that increasing the inserted urethane group, which destroy the regularity of polymer chains, bring a sharply reduce of crystallization rate of copolymers.

Not only the urethane group content should influence the crystallization behavior of products but also the OMMT content in the nanocomposites plays dominant role in the process. Figure 10 shows the spherulite growth rate of $PPDO_{40}$-PU/OMMT ([η]=1.4∼1.6 dL/g) at different isothermal crystallization temperature. Compared with unloaded $PPDO_{40}$-PU, the spherulite growth rate of $PPDO_{40}$-PU/1%OMMT and $PPDO_{40}$-PU/3%OMMT decreased evidently. It suggests that exfoliated OMMT platelets did not act as a template for the spherulite growth process; on the contrary, they impeded PPDO molecular chains to arrange regularly and form spherulites more slowly. The POM observation quite coincided with the results from DSC analysis.

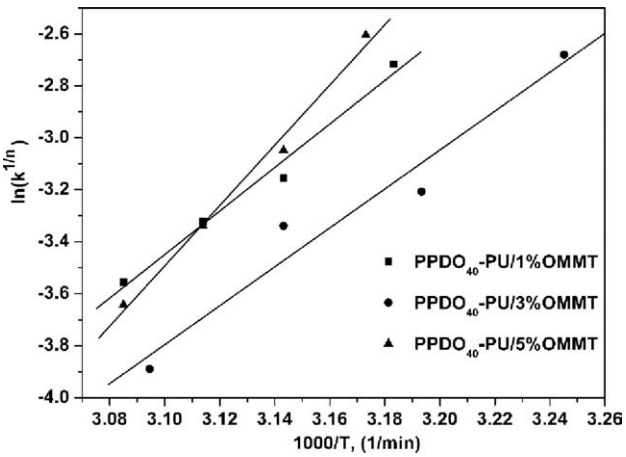

Figure 7. Plot of ln $k^{1/n}$ versus $1/T_c$.

CONCLUSION

The crystallization behavior and spherulitic morphology of PPDO-PU/OMMT nanocomposites prepared by chain-extending reaction were disclosed by WXRD, DSC, and POM in detail. In all, the insertion of urethane groups depressed the crystallizability of PPDO-PU/OMMT nanocomposites. The regularity of the chain structure was proved to play a dominant role during the crystallization process rather than that of OMMT content and its dispersion in PPDO matrix. With similar molecular weight and same OMMT content, therefore, PPDO-PU/OMMT nanocomposites with higher urethane group content exhibited lower crystallization rate, lower melting point, and lower crystallinity. The influence of the clay on the crystallization behavior highly depends on its dispersing state. The nucleating effect of OMMT only could be observed at high loading percentage. The nanocomposites with low clay loading percentage, PPDO-PU/1%OMMT and PPDO-PU/3%OMMT, showed lower crystallization rate than the unloading one, which informed that the retarding effect of exfoliated platelets on the chain-ordering into crystal lamellae became the key factor.

ACKNOWLEDGMENTS

Contract grant sponsor: National Science Foundation of China; contract grant number: 50873064. Contract grant sponsor: Funds for Young Scientists of Sichuan Province, China; contract grant number: 2010JQ0015. Contract grant sponsor: Program of

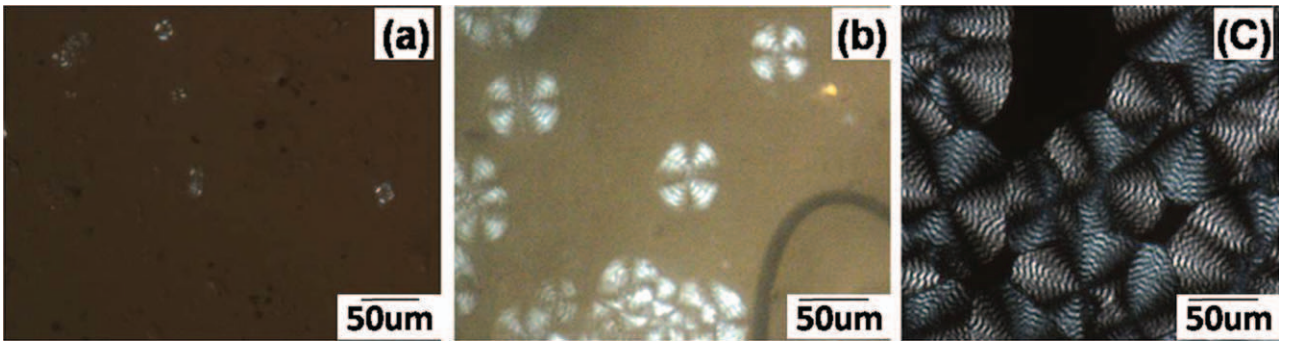

Figure 8. Spherulitic morphology of PPDO-PU/3%OMMT: (a) $PPDO_{20}$-PU/3%OMMT; (b) $PPDO_{40}$-PU/3%OMMT; and (c) $PPDO_{100}$-PU/3%OMMT (temperature: 50°C, time: 8 min). [Color figure can be viewed in the online issue, which is available at wileyonlinelibrary.com.]

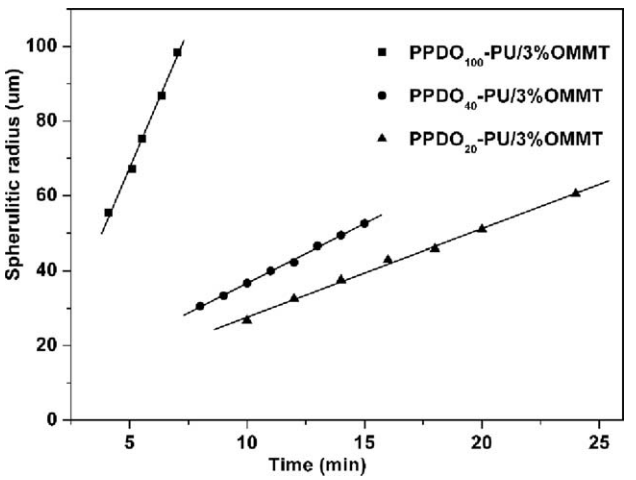

Figure 9. The linear relationship between spherulitic diameter and crystallization time of different PPDO-PU/3%OMMT at 50°C.

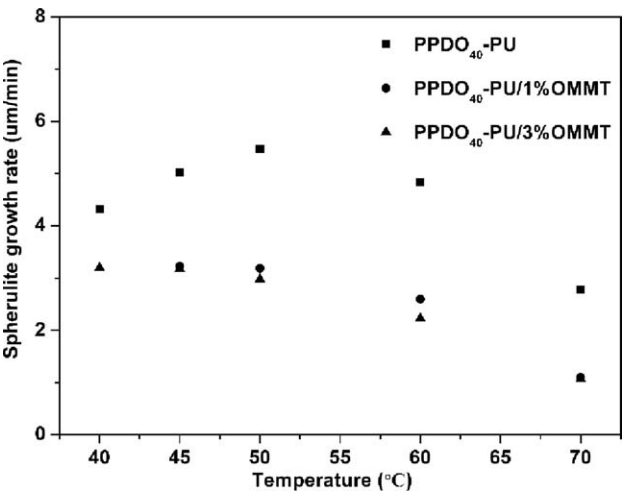

Figure 10. Spherulite growth rate of different $PPDO_{40}$-PU/OMMT with different OMMT content at different crystallization temperature.

International S & T Cooperation; contract grant number: 2011DFA51420. Contract grant sponsor: Program for Changjiang Scholars and Innovative Research Team in University of Ministry of Education of China; contract grant number: IRT1026.

REFERENCES

1. Suzuki, A.; Terai, H.; Toyoda, H.; Namikawa, T.; Yokota, Y.; Tsunoda, T.; Takaoko, K. *J. Orthop. Res.* **2006,** *24*, 327.
2. Blanco, M. G.; Franco, L.; Puiggalí, J.; Rodríguez-Galán A. *J. Appl. Polym. Sci.* **2009,** *114*, 3440.
3. Yomeda, M.; Terai, H.; Imai, Y.; Okada, T.; Nozaki, K.; Inoue, H.; Miyamoto, S.; Takaoka, K. *Biomaterials* **2005,** *26*, 5145.
4. Yang, K. K.; Wang, X. L.; Wang, Y. Z. *J Macromol. Sci. Polym. Rev.* **2002,** *C42*, 373.
5. Bergamaschi, J. M.; Pilau, E. J.; Gozzo, F. C.; Felisberti M. I. *Macromol. Symp.* **2011,** *299/300*, 10.
6. Toyoda, H.; Terai, H.; Sasaoka, R.; Oda, K.; Takaoko, K. *Bone* **2005,** *37*, 555.
7. Zeng, J. B.; Srinivansan, M.; Li, S. L.; Narayan, R.; Wang, Y. Z. *Ind. Eng. Chem. Res.* **2011,** *50*, 4471.
8. Ding, S. D.; Zheng, G. C.; Zeng, J. B.; Zhang, L.; Li, Y. D.; Wang, Y. Z. *Eur. Polym. J.* **2009,** *45*, 3043.
9. Chen, F.; Chen, S. C.; Yang, K. K.; Wang, X. L.; Wang, Y. Z. *Eur. Polym. J.* **2010,** *46*, 24.
10. Zhu, J.; Dong, X. T.; Wang, X. L.; Wang, Y. Z. *Carbohydr. Polym.* **2010,** *80*, 350.
11. Wang, X. L.; Huang, Y.; Zhu, J.; Pan, Y. B.; He, R.; Wang, Y. Z. *Carbohydr. Res.* **2009,** *344*, 801.
12. Wang, X. L.; Mou, Y. R.; Chen, S. C.; Shi, J.; Wang, Y. Z. *Eur. Polym. J.* **2009,** *45*, 1190.
13. Chen, R.; Hao, J. Y.; Xiong, C. D.; Deng, X. M. *Adv. Eng. Mater.* **2010,** *12*, B504.
14. Rodríguez-galán, A.; Franco, L.; Puiggalí, J. *J. Polym. Sci. Part A: Polym. Chem.* **2009,** *47*, 6758.
15. Wu, G.; Chen, S. C.; Zhan, Q.; Wang, Y. Z. *J. Polym. Sci. Part A: Polym. Chem.* **2010,** *48*, 4811.
16. Lu, F.; Wang, X. L.; Chen, S. C.; Yang, K. K.; Wang, Y. Z. *J. Polym. Sci. Part A: Polym. Chem.* **2009,** *47*, 5344.

17. Remant Bahadur, K. C.; Aryal, S.; Bhattarai, S. R.; Khil, M. S.; Kim, H. Y. *J. Appl. Polym. Sci.* **2007,** *103*, 2695.
18. Huang, H. X.; Yang, K. K.; Wang, Y. Z.; Wang, X. L.; Li, J. *J. Polym. Sci. Part A: Polym. Chem.* **2006,** *44*, 1245.
19. Li, F.; Feng, J.; Zhuo, R. X. *J. Appl. Polym. Sci.* **2006,** *102*, 5507.
20. Remant Bahadur, K. C.; Bhattarai, S. R.; Aryal, S.; Khil, M. S.; Dharmaraj, N.; Kim, H. Y. *Colloids Surf. A: Physicochem. Eng. Aspects* **2007,** *292*, 69.
21. Jiang, Z. Z.; Azim, H.; Gross, R. A. *Biomacromolecules* **2007,** *8*, 2262.
22. Andjelic, S.; Jamiolkowski, D. D.; Kelly, B. M.; Newman, H. *Macromolecules* **2003,** *36*, 8024.
23. Yang, K. K.; Zheng, L.; Wang, Y. Z.; Zeng, J. B.; Wang, X. L.; Chen, S. C.; Zeng, Q.; Li, B. *J. Appl. Polym. Sci.* **2006,** *102*, 1092.
24. Hong, J. T.; Cho, N. S.; Yoon, H. S.; Kim, T. H.; Koh, M. S.; Kim, W. G. *J. Appl. Polym. Sci.* **2006,** *102*, 737.
25. Li, Y. D.; Chen, S. C.; Zeng, J. B.; Wang. Y. Z. *Ind. Eng. Chem. Res.* **2008,** *47*, 8233.
26. Wu, G.; Chen, S. C.; Zhan, Q.; Wang, Y. Z. *Macromolecules* **2011,** *44*, 999.
27. Giammanco, G.; de Ilarduya, A. M.; Alla, A.; Munoz-Guerra, S. *Biomacromolecules* **2010,** *11*, 2512.
28. He, R.; Wang, X. L.; Wang, Y. Z.; Yang, K. K.; Zeng, J. B.; Ding, S. D. *Carbohydr. Polym.* **2006,** *65*, 28.
29. Li, B.; Chen, S. C.; Qiu, Z. C.; Yang, K. K.; Tang, S. P.; Yu, W. J.; Wang, Y. Z. *Polym. Bull.* **2008,** *61*, 139.
30. Zhang, Y. H.; Wang, X. L.; Wang, Y. Z.; Yang, K. K; Li, J. *J. Polym. Degrad. Stab.* **2005,** *88*, 294.
31. Lai, Q.; Wang, Y. Z.; Yang, K. K.; Wang, X. L.; Zeng, Q. *React. Funct. Polym.* **2005,** *65*, 309.
32. Yang, K. K.; Zeng, Q.; Wang, X. L.; Zhu, X. L.; Zhou, Y.; Wang, Y. Z. Chem. J. *Chinese U* **2007,** *11*, 2190.
33. Zeng, Q.; Yang, K. K.; Chen, S. C.; Wang, X. L.; Zeng, J. B.; Wang, Y. Z. *Eur. Polym. J.* **2008,** *44*, 465.
34. Zhou, Y.; Qiu, Z. C.; Zhang, J. J.; Niu, Y.; Yang, K. K.; Wang, Y. Z. *Soft Mater.* **2011,** *9*, 393.
35. Bai, W.; Zhang, L. F.; Li, Q.; Chen, D. L.; Xiong, C. D. *Mater. Chem. Phys.* **2010,** *122*, 79.
36. Brito, Y.; Sabino, M. A.; Ronca, G.; Müller. A. J. *J. Appl. Polym. Sci.* **2008,** *110*, 3848.
37. Lu, J. M.; Qiu, Z. B.; Yang, W. T. *Polymer* **2007,** *48*, 4196.
38. Zeng, J. B.; Zhu, Q. Y.; Li, Y. D.; Qiu, Z. C.; Wang, Y. Z. *J. Phys. Chem.* **2010,** *114*, 14827.
39. Pezzin, A. P. T.; Duek, E. A. R. *J. Appl. Polym. Sci.* **2006,** *101*, 1899.
40. Zhou, Y.; Zhang, J. J.; Qiu, Z. C.; Zeng, Q.; Chang, J. J.; Yang, K. K.; Wang, Y. Z. *Soft Mater.* **2009,** *7*, 277.
41. Huang, F. Y.; Wang, Y. Z.; Wang, X. L.; Yang, K. K.; Zhou, Q.; Ding, S. D. *J. Polym. Sci. Part A: Polym. Chem.* **2005,** *43*, 2298.
42. Wang, C.; Ge, X. G.; Yang, K. K.; Chen, S. C.; Wang, Y. Z. *Soft Mater.* **2009,** *7*, 116.
43. Yang, K. K.; Zhou, Y.; Lu, F.; Huang, F. Y.; Qiu, Z. C.; Wang, Y. Z. *J. Macromol. Sci. Phys.* **2009,** *48*, 1031.
44. Qiu, Z. C.; Zhang, J. J.; Zhou, Y.; Song, B. Y.; Chang, J. J.; Yang, K. K.; Wang, Y. Z. *Polym. Adv. Technol.* **2009,** *22*, 993.
45. Zubitur, M.; Fernández, A.; Mugica, A.; Cortázar, M. *Phys. Stat. Sol.* **2008,** *205*, 1515.
46. Zubitur, M.; Mugica, A.; Areizaga, J.; Cortázar, M. *Colloid. Polym. Sci.* **2010,** *288*, 809.
47. Avrami, M. *J. Chem. Phys.* **1939,** *7*, 1103.
48. Ishikiriyama, K.; Pyda, M.; Zhang, G., Forschner, T.; Grebowicz, J.; Wunderlich, B. *J. Macromol. Sci. Phys.* **1998,** *B37*, 27.